

Structure and dynamics in hexagonal ice: A molecular dynamics simulation with an *ab initio* polarizable and flexible potential

Francesco Sciortino and Giorgina Corongiu

CRS4, Centro di Ricerca, Sviluppo e Studi Superiori in Sardegna, P.O. Box 488, 09100 Cagliari, Italy

(Received 15 June 1992; accepted 9 December 1992)

We perform a molecular dynamics simulation of the hexagonal solid phase of water, using a new polarizable and flexible potential which has been derived from quantum mechanical calculations. We calculate and compare with available experimental data the molecular structure, the density of states in the translational, librational, and vibrational regions as well as the acoustic dispersion relations. The molecular structure in the condensed phase is found to be in agreement with the recent interpretation of the neutron scattering data of Kuhs and Lehmann [W. F. Kuhs and M. S. Lehmann, *J. Phys. (Paris)* **48**, C1, 3 (1987)]. The collective low frequency modes in the simulated ice are in good agreement with the experimental data in the *c*-axis direction but 20% softer in the hexagonal plane.

I. INTRODUCTION

In the last few years many new potentials have been proposed to model water–water interactions.^{1–3} The availability of computers with large memory and fast processing units has made possible to step from the previous two-body description of molecular interactions to more complex many-body descriptions. This is particularly relevant in the case of assemblies of water molecules, where polarization contributions make up a significant part of the total binding energy.

The new many-body potentials should be suitable to describe successfully all phases of water: the gas phase, the liquid phase, and the many forms of ice. Indeed, one of the major goals of these potentials should be to give the possibility to study phase transitions, interphases, water close to biomolecules, etc., within a unifying framework, i.e., without choosing an *ad hoc* potential for each specific application.

Two classes of many-body potentials have been developed to describe the water–water interactions: (i) the class of empirical potentials, where the parameters in the analytic form of the potential energy are parametrized against experimental data and (ii) the class of *ab initio* potentials, where the parameters are determined on the basis of quantum mechanical calculations on small clusters of water molecules.

Among the second class, one polarizable potential has been developed by Nieser, Corongiu, and Clementi (NCC in the following)¹ and successfully applied to study the static and dynamics properties of water in the gas and liquid phases. This potential, parametrized against quantum mechanical calculations at the MP4 level for water dimers and at the HF level for water trimers,¹ is composed by two contributions: a two-body potential, $E_{\text{two-body}}$, and a polarization term, E_{pol} . The polarization effects in the NCC potential are represented by a point polarizability along the two OH bonds. For more detail see Ref. 1. An intramolecular term, E_{intra} , has been recently added to the NCC potential to take into account the intramolecular degrees of freedom. This new model potential, which we will refer to

as NCC–vib, has been applied to study liquid water in a wide range of temperatures.⁴

The aim of this paper is to assess the reliability of the *ab initio* NCC–vib potential in describing the structure and the dynamics of hexagonal ice (I_h). We focus on (i) the intramolecular and intermolecular structure, a subject of long standing debate;⁵ (ii) the density of states (DOS), the frequency distribution of the *atomic* motions; and (iii) the dispersion relation of the acoustic modes, which probes the *collective* dynamical behavior of the system.

II. COMPUTATIONAL DETAILS

We have performed molecular dynamics (MD) simulation on a system of 432 deuterated water molecules confined in a rectangular box and interacting through the *ab initio* polarizable and flexible NCC–vib potential.¹

The simulation has been carried out at constant energy and constant density (NVE ensemble). Periodic boundary conditions have been applied to simulate the infinite system and the Ewald summation has been used to handle the electrostatic interactions. The self-consistent set of induced dipole moments was calculated by an iterative method, as explained in detail in Ref. 1. A sixth-order Gear predictor corrector method was used to integrate the equations of motion with a time step of 0.15 femtoseconds. The simulation has been conducted for a total of 60 ps. The equilibration phase required 20 ps with rescaling of the particle velocities. The additional 40 ps were carried out without any velocity rescaling and used to collect statistical properties. During the last 40 ps we dumped into a disk the coordinates and velocities of all particles every 1.35 fs. The average temperature, computed from the average kinetic energy of the system, was 100 K. The total energy is conserved during the run within 0.005 kJ/mol.

In the I_h structure the oxygen atoms are tetrahedrally coordinated via hydrogen bonds (HB) with a disordered arrangement of the proton. The starting crystalline structure of our simulation was obtained by placing the oxygen atoms in a perfect tetrahedral structure. The protons were

TABLE I. Molecular dynamics data for the simulation under discussion. \pm values indicate standard deviation.

System	D ₂ O
Density (mol/l)	52.1
Temperature (K)	99.7 \pm 1.6
Pressure (MPa)	-30.8 \pm 6.7
$E_{\text{kin+pot}}$ (kJ/mol)	-53.6
$E_{\text{two-body}}$ (kJ/mol)	-32.8 \pm 0.1
E_{pol} (kJ/mol)	-28.7 \pm 0.1
E_{intra} (kJ/mol)	4.1 \pm 0.1
μ (Debye)	3.3 \pm 0.1

then positioned in such a way to satisfy the ice rules and to yield a proton disordered periodic structure with zero net dipole moment.⁶

III. STATIC PROPERTIES

Table I summarizes some information on the MD simulation under discussion. First we note that a large fraction of the cohesive energy arises from the polarization term (about 50%). The ratio between the two-body and the polarization contribution ($E_{\text{two-body}}/E_{\text{pol}}=1.14$) is slightly smaller than the value found in the simulation of the liquid phase ($E_{\text{two-body}}/E_{\text{pol}}=1.35$). The pressure of the system is negative, as found in the simulation of the liquid phase.¹ As discussed in more detail in Ref. 1, such a negative value could originate from a too weak representation of the short distance repulsion and/or from the inaccuracies associated with the classical, rather than quantum molecular dynamics simulation. Indeed, the quantum delocalization of the protons, fully taken into account by quantum simulations (for example, by using the path integral Monte Carlo method), would increase the sampling in the highly repulsive regions of the potential with a corresponding increase of the average pressure in the system.

The average molecular dipole at 100 K is 3.3 Debye. This value has to be compared with equivalent quantities obtained with the same potential: 1.85 D for one water molecule in the gas phase and 2.8 D and 3.1 D for the liquid phase, at $T=305$ K and $T=242$ K, respectively. The variance of the dipole distribution is rather small, even if the proton disorder differentiates the local molecular configurations.

The molecular dipole is related to the dielectric constant by the Kirkwood correlation parameter, g_k , and by the value of the internal field acting on a water molecule. Extensive work in the last two decades seems to suggest $g_k=3$ as an upper limit value of the I_h structure.⁷ Regarding the internal field, an upper limit value is given by the Lorenz field, while a lower limit can be calculated by assuming that the internal field coincides with the applied field. By using $g_k=3$ and the experimental dielectric constant value, the two extreme values for the internal field give a value for μ between 2.45 and 3 D.⁷ Then, the NCC-vib potential seems to give a dipole moment about 10% larger than the value suggested by the experiment.

The statistical distribution of the intramolecular degrees of freedom, as obtained from our simulation, i.e., the

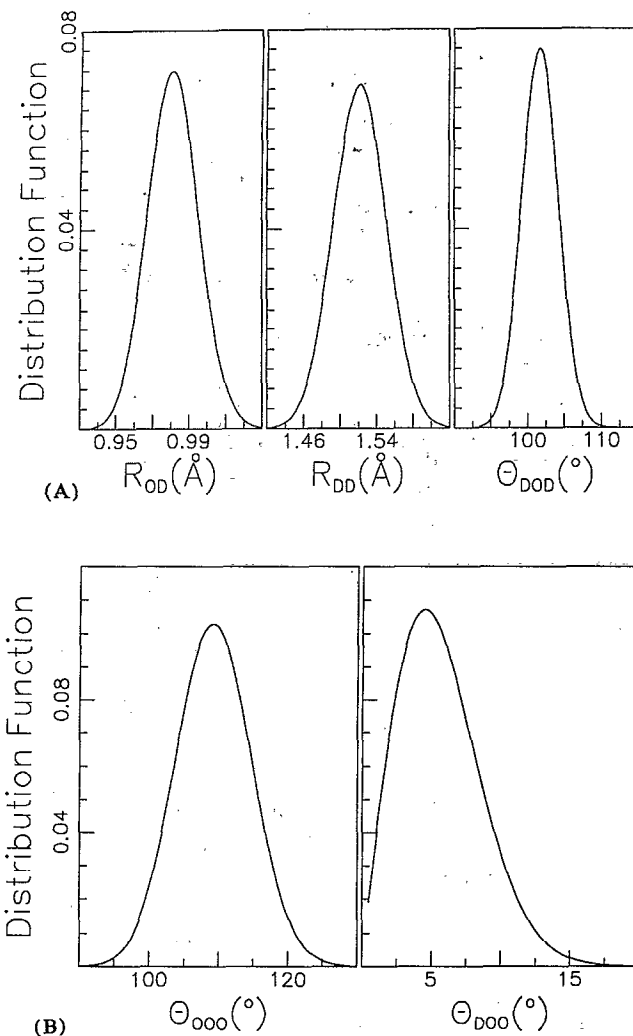


FIG. 1. (A) Statistical distribution for the OD and DD bond lengths, R_{OD} , R_{DD} , and for the DOD bond angle Θ_{DOD} . (B) Statistical distributions for the deuterium-oxygen-oxygen angle Θ_{DOO} and for the oxygen-oxygen-oxygen angle Θ_{OOO} . Only first neighbors are taken into account to evaluate Θ_{DOO} and Θ_{OOO} .

OD and DD bond lengths (R_{OD} and R_{DD} in the following), and the DOD bond angle Θ_{DOD} , is shown in Fig. 1. Also reported in the same figure are the distributions for the deuterium-oxygen-oxygen angle Θ_{DOO} , a measure of the hydrogen bond linearity, and for the oxygen-oxygen-oxygen angle Θ_{OOO} , a measure of the tetrahedrality of the lattice formed by the oxygens atoms. Only first neighbors are taken into account to evaluate Θ_{DOO} and Θ_{OOO} . As well known, in the absence of any coupling between velocity and position in the potential energy, the structural properties are independent from the mass of the atoms; therefore, the static properties calculated from our classical MD simulation refer both to D₂O and H₂O.

The calculated average R_{OD} value, 0.981 Å, is longer than the corresponding gas phase value of 0.9572 Å and only slightly longer (of 0.003 Å) than the OD distance found in a simulation, using the same potential, for the liquid phase at $T=242$ K.⁴

The calculated Θ_{DOD} angle decreases from the gas

phase value of 104.6° to 101.7° , a slightly smaller decrease compared with the change in Θ_{DOD} from 104.6° to 100.8° found in the NCC-vib simulation of the liquid state at $T=242$ K.

The geometry of the water molecule in the solid phase was previously considered as fairly well understood.⁸⁻¹⁰ High resolution neutron diffraction experiments for the ice I_h phase⁹ suggested a OD length of 1.01 Å and a DOD angle of 109.5° . These unusual bond lengths and angle in the molecule have been questioned by Whalley on the basis of Raman and NMR data¹⁰ and by Chidambaran.¹¹ Indeed, the OH distance of 1.01 Å is considerably longer than the 0.97 Å value normally found for bound water in crystalline compounds. Also the HH distance, 1.62 Å, suggested by the analysis of the neutron experiments^{8,9} is longer than the HH value of 1.58 Å extracted by NMR data.¹⁰

Over the last few years, the view of the ice I_h has changed considerably.¹² Neutron data, reinterpreted taking into account the existence of disorder in the oxygen atom positions, are now in much closer agreement with the results from all the other experimental techniques. The currently best estimate for the O-H(D) bond length is $R_{\text{OH}}=0.987(5)$ Å and $R_{\text{OD}}=0.983(5)$ Å.¹² Combining the $R_{\text{OH}}=0.987(5)$ Å value with the adopted NMR H-H distances of $1.58(1)$ Å one obtains an intramolecular angle of 107° .

By comparing our numerical results with the distances quoted above we conclude that the NCC-vib potential gives the correct bond length but a too narrow bond angle. We also note that an even larger narrowing ($\Theta_{\text{HOH}}=101.0^\circ$) has been observed in an independent simulation of hexagonal ice with a different potential.¹³ The narrowing of the bond angle and the overestimated value for the dipole moment seem to indicate that the NCC-vib potential overestimates the polarization effect along the hydrogen bonds. Indeed the values for the transverse and the longitudinal polarization in the NCC-vib model are 15% greater than the experimental values.¹⁴

It is worth noting that also the geometry of the water molecule in the liquid state is not fully established from an experimental point of view. The two most reliable sets of experimental data in literature^{15,16} give contradictive results for the HH distance and the Θ_{HOH} values. The calculated quadratic mean displacement, a measure of the delocalization of the atoms in the solid, is 0.155 Å for the oxygens atoms and 0.165 Å for the deuterium atoms. These values are in very good agreement with the neutron data values⁹ of 0.15 Å for the oxygen and 0.16 – 0.20 Å for the hydrogen atoms for a sample at $T=123$ K.

The oxygen lattice, as shown by the Θ_{OOO} distribution function (see Fig. 1), is tetrahedrally coordinated, with an average Θ_{OOO} angle of 109.2° very close to the perfect tetrahedral value. The deuterium atoms involved in the HBs are in average off the OO bond line by 4° , a result consistent with the difference between the Θ_{OOO} and the Θ_{DOD} angles. It is worth pointing out that the equilibrium structure in water dimers is already characterized by a slight nonlinear HB.

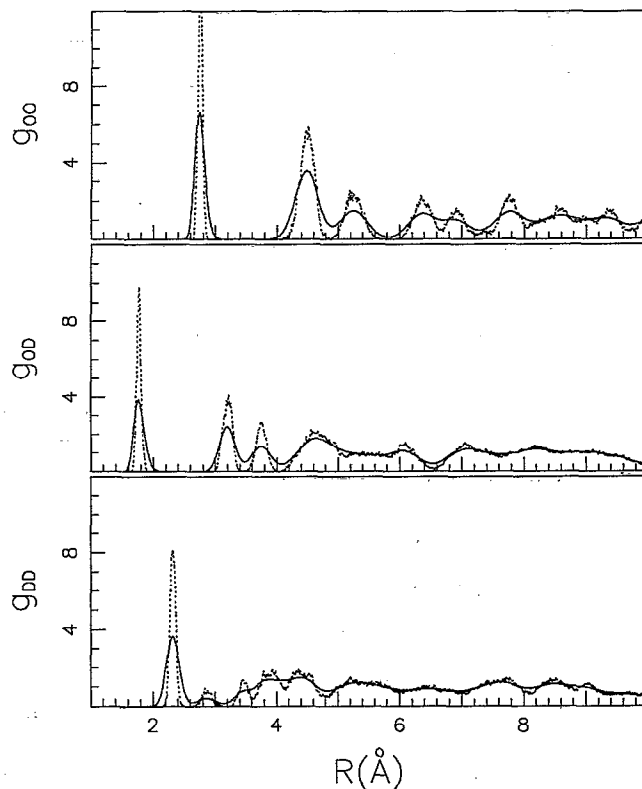


FIG. 2. Oxygen-oxygen (g_{OO}), oxygen-deuterium (g_{OD}), and deuterium-deuterium (g_{DD}) radial distribution functions. $T=100$ K (full line) and $T=0$ K (dashed line).

Figure 2 shows the intermolecular OO, OD, and DD radial distribution functions [$g(r)$]. The $g(r)$ calculated for the ice I_h structure at $T=100$ K are drawn as full lines. The broken lines refer to the $g(r)$ functions calculated for the same system after an energy minimization ($T=0$ K). We observe that the disorder connected with the proton positions affects significantly also the oxygen positions and broadens the distributions for intermolecular OO and OD distances. We find that the first neighbors OO distance at $T=0$ K (i.e., when only positional disorder is taken into account) has a spread of 0.02 Å. Refined neutron data yield for the same quantity values of a few hundredths of one angstrom.¹²

IV. DYNAMICAL PROPERTIES: TRANSLATIONAL REGION

The density of states (DOS), a measure of the number of modes available to the atoms in the system at frequency ω , can be obtained from the Fourier transform of the oxygen (or deuterium) atom velocity autocorrelation function:

$$\text{DOS}(\omega) = \int_0^\infty \exp(-i\omega t) \langle \mathbf{V}(t) \cdot \mathbf{V}(0) \rangle / \langle \mathbf{V}(0) \cdot \mathbf{V}(0) \rangle dt.$$

In the hindered translation region the density of states of the deuterium and oxygen atoms is similar in shape and intensity, since the component of the velocity associated

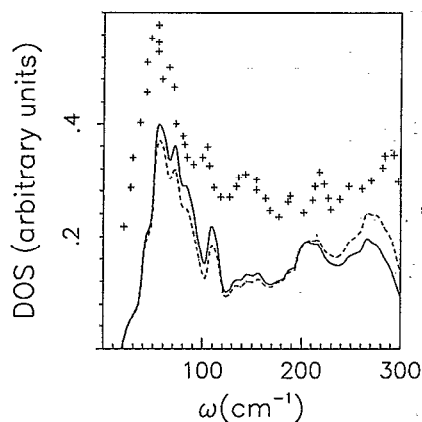


FIG. 3. Density of states of the deuterium (full line) and oxygen (dashed line) atoms in ice I_h . The + signs refer to the low frequency incoherent inelastic neutron scattering data of Ref. 17.

with all translational modes are the same for both types of atoms. This fact, along with the large incoherent scattering length of the protons, enables, for water, the experimental measure of an effective DOS in the translation region.

In Fig. 3 we report, for the region 0–300 cm^{-1} , the calculated DOS for deuterium and oxygen atoms and we compare it with the new inelastic incoherent neutron experimental (IINS) results from Ref. 17. Both set of data show several peaks, which correspond to the acoustic and optic modes of the crystal. We observe that the NCC-vib DOS very well reproduces the regions below 100 and above 150 cm^{-1} , but fails to reproduce the correct position of the peaks in the region between 100 and 150 cm^{-1} . To identify the acoustic peaks and to trace back the possible sources of disagreement between experimental and simulated data in the intermediate frequency region, we study the dispersion relation for the low-frequency modes. To discriminate between longitudinal and transverse modes, we have calculate the longitudinal and transverse particle current $\mathbf{J}(\mathbf{r}, t)$ for some directions in the Brillouin space. $\mathbf{J}(\mathbf{r}, t)$ is defined as¹⁸

$$\mathbf{J}(\mathbf{r}, t) = \sum_{i=1}^N \mathbf{u}_i(t) \delta[\mathbf{r} - \mathbf{r}_i(t)]$$

and its space Fourier transform

$$\mathbf{J}_\mathbf{k}(t) = \sum_{i=1}^N \mathbf{u}_i(t) \exp[-i\mathbf{k} \cdot \mathbf{r}_i(t)],$$

where \mathbf{u}_i and \mathbf{r}_i are, respectively, the velocity and the position of particle i , and N the total number of atoms. The Fourier components can be separated into longitudinal and transverse components, parallel and perpendicular, respectively, to the wave vector \mathbf{k} . The position of the peaks in $\mathbf{J}_\mathbf{k}(\omega)$, the spectral density of $\mathbf{J}_\mathbf{k}(t)$, enables to determine the frequency-wave vector relations for the transverse and longitudinal acoustic phonons in our system.

We have also calculated the dynamical structure factor, $S(\mathbf{k}, \omega)$, defined as the time Fourier transform of the intermediate scattering function.¹⁸ This quantity was used in a previous study of the collective excitations in I_h .¹⁹ As

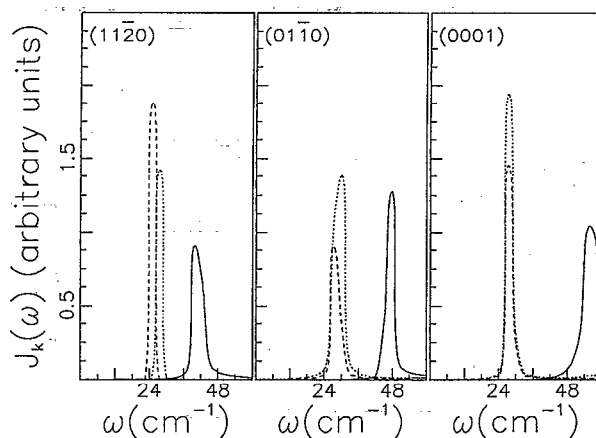


FIG. 4. Longitudinal (full line) and transverse (dashed and dotted lines) particle current $\mathbf{J}_\mathbf{k}(\omega)$ for the directions (0001), (1120), (0110) at $k=0.2335, 0.2697, \text{ and } 0.2861 \text{ \AA}^{-1}$, respectively.

in the $S(\mathbf{k}, \omega)$ data reported in Ref. 19, the amplitude of the peaks of the transverse excitations that we observe in $S(\mathbf{k}, \omega)$ is very close to the noise level and, differently from the $\mathbf{J}_\mathbf{k}(\omega)$ curves, does not allow a clear determination of the transverse dispersion curves.²⁰

We have calculated $\mathbf{J}_\mathbf{k}(\omega)$ along three directions in \mathbf{k} space, (0001), (1120), (0110), which correspond in real space to the c -axis direction and to two directions perpendicular to the c axis. On the hexagonal lattice the directions (1120) and (0110) correspond to the two lines connecting first and second neighbors, respectively. The crystal symmetries allow us to average $J_\mathbf{k}(\omega)$ with respect to \mathbf{k} vectors with the same magnitude.

In Fig. 4 we show the spectral density of the longitudinal and transverse particle current for the smallest wave vectors \mathbf{k} (imposed by our box dimension) in the three considered directions. We observe very sharp peaks at the acoustic phonon frequencies. The dispersion relationships for the three studied directions are shown in Fig. 5. Also reported in this figure are the experimental points from Ref. 21. The corresponding acoustic velocities, obtained as the ratio of frequency and wave vector for the smallest \mathbf{k} value available for each direction, are, respectively, 2.1, 2.1, and 2.0 Km/s for the transverse modes and 3.3, 3.4 and 3.8 Km/s for the longitudinal modes, to be compared with the experimental values, for polycrystalline ice I_h , of 2.0 and 3.9 Km/s.²²

The agreement between simulated and experimental data is very good in the (0001) direction (c axis) and for the transverse phonons in the (1120) and (0110) directions. Less satisfactory are the results for the acoustic longitudinal phonons, whose values are in general 10–20 % smaller than the corresponding experimental data.

By comparing, for the three studied directions, the positions of the peaks in the DOS (Fig. 3) with the dispersion relations at the zone boundaries (Fig. 5), we associate: (i) the (0–100 cm^{-1}) region with the well reproduced transverse acoustic modes; (ii) the (100–140 cm^{-1}) region with the longitudinal acoustic modes in the (1120) and (0110)

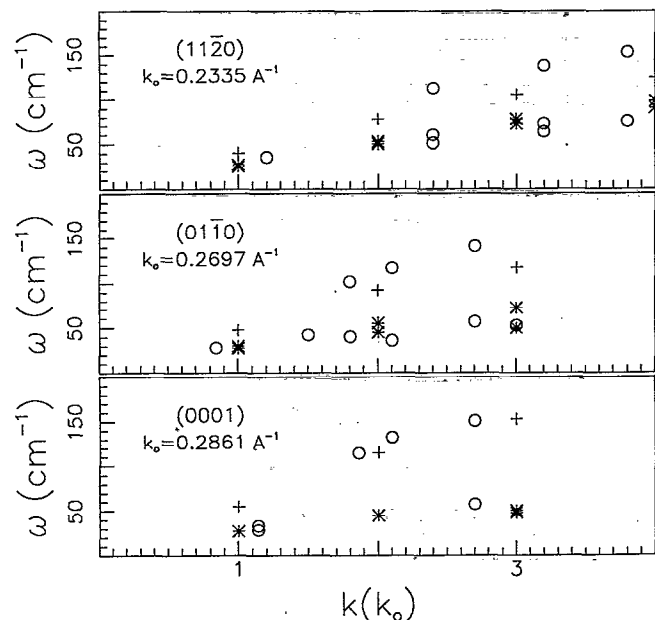


FIG. 5. Dispersion relations for the longitudinal (pluses) and transverse (stars) acoustic modes in the (0001), (1120), (0110) directions. Note that the crystallographic point K coincides with $k=4k_0$ in the (1120) direction, the point M with $k=3k_0$ in the (0110) direction, and the point A with $k=1.5k_0$ in the (0001). The calculated frequencies are compared with the coherent inelastic neutron scattering data (circles) of Ref. 21. The k_0 value for each direction is also shown in the figure.

directions; (iii) the region around 160 cm^{-1} with the longitudinal acoustic modes in the (0001) direction. The remaining peaks in the DOS are associated with optical modes. We recall that in the region $100\text{--}140\text{ cm}^{-1}$ we find disagreement between the computed and the experimental DOS.

While in the c -axis direction, the longitudinal modes are mainly of OO stretching character, in the hexagonal plane the modes have a substantial OOO bending character. We are then led to conclude that the surface of the NCC-vib potential reproduces very closely the curvature of the energy surface for the real system in the OO direction, but that there is space for further improvement in the more sensitive region of the potential hypersurface that controls the OOO bending modes.

V. DYNAMICAL PROPERTIES: LIBRATIONAL REGION

Figure 6 compares, for the deuterium atoms, the calculated DOS with the recent inelastic incoherent neutron experimental results from Refs. 17 and 23, in the region $300\text{--}800\text{ cm}^{-1}$. In this frequency region, the spectra are dominated by the rotational motion of the water molecules. The calculated spectrum reproduces fairly well the overall shape and width of the experimental librational band, but is shifted toward low frequencies by about 50 cm^{-1} . A clear separation in two domains is seen in both set of data, with a minimum at about 490 cm^{-1} in the simulated spectrum and at 540 cm^{-1} in the IINS spectrum. A large number of secondary maxima and minima is observed in the

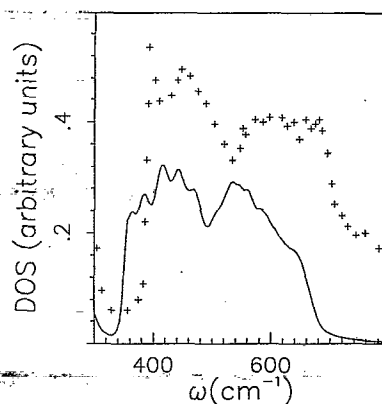


FIG. 6. Deuterium atom density of states in the librational region for Ice I_h (full line) compared with the low frequency incoherent inelastic neutron scattering data of Ref. 17 (pluses).

calculated spectrum, which we attribute to the finite number of local configurations used in the calculation. Indeed, preliminary tests with smaller system sizes showed an even larger number of such secondary maxima.

The agreement between simulated and experimental data is significant, especially if we compare the present spectrum with the one evaluated for the MCY, the SPC, and the TIPS2 potentials (see Fig. 2 in Ref. 19). Recalling that all those potentials are at the two-body level, the comparison points out the importance of the many-body terms in the water-water potential, from which the shape of the energy hypersurface and the dynamics of the water molecules depend.

VI. DYNAMICAL PROPERTIES: VIBRATIONAL REGION

In Fig. 7 we report in a semilog scale the density of states between 0 and $12\,000\text{ cm}^{-1}$. Note that molecular dynamics is a unique technique for providing detailed in-

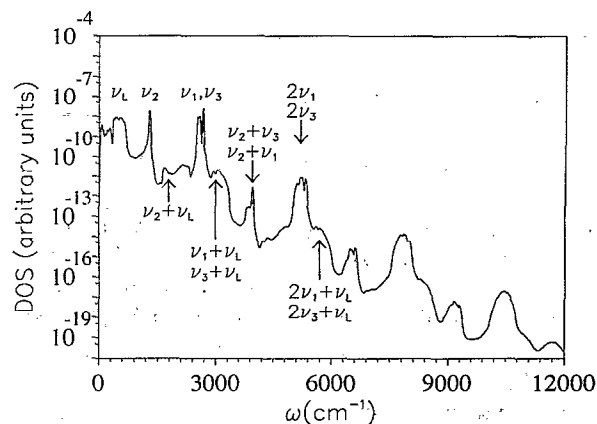


FIG. 7. Deuterium atom density of states for ice I_h in a semilog scale. Note that very scarcely populated overtones can be detected via analysis of MD data. Some of the fundamental frequencies and the first overtones have been explicitly indicated in the figure: $\nu_2=1284\text{ cm}^{-1}$, $\nu_1=2550\text{ cm}^{-1}$, $\nu_3=2670\text{ cm}^{-1}$.

formation on molecular modes covering an intensity range of more than 12 orders of magnitude.

The region 0–800 cm^{-1} , which covers the translational and librational modes, has been discussed in the previous sections. Here, we focus on the vibrational region, which gives information on the fundamental modes (bending and stretching) but also on the weaker overtones and combination modes populated at the present temperature.

In Fig. 7 we notice peaks with high intensity occurring at $\sim 1285 \text{ cm}^{-1}$, $\sim 2550 \text{ cm}^{-1}$ and $\sim 2670 \text{ cm}^{-1}$, which must be associated, respectively, with the bending, the symmetric and the asymmetric stretching modes. By comparing the calculated frequencies with experimental values,²⁴ we find that the simulation results are overestimated by $\sim 85 \text{ cm}^{-1}$ for the bending and $\sim 250 \text{ cm}^{-1}$ for the stretching mode. Equivalent deviations have been found for simulations of the liquid state¹ using the same potential. However, the value of the bending mode, ν_2 , in the simulated I_h phase up-shifts by about 50 cm^{-1} with respect to the gas phase value calculated with the same potential. Such up-shift is consistent with the experimentally observed change on going from the gas to the solid phase. Moreover, the value of ν_2 in the I_h phase coincides with the value found in the simulation of the liquid phase,¹ again in agreement with the experimental absence of a shift on going from the liquid to the solid phase.

The position of the stretching modes, ν_1 and ν_3 , is instead down-shifted with respect to the computed liquid and gas phase values, again in agreement with the experimental findings. We also observe a clear splitting of ν_1 and ν_3 of about 120 cm^{-1} , to be compared with the recently observed^{17,23} experimental splitting value of 130 cm^{-1} .

Between the bending and the stretching frequencies, we observe (see Fig. 7) a weaker signal which can be attributed, from its width and position, to the combination of the librational and bending modes ($\nu_2 + \nu_L$) (see also Ref. 23). Immediately before the ν_1 peak we can notice a large band, which we associate to the two combination bands ($\nu_1 - \nu_L$) and ($\nu_3 - \nu_L$). Above the stretching frequencies we observe, with decreasing amplitude, combinations and overtones of the librational and vibrational modes; Fig. 7 clearly shows the combination of libration and vibrations ($\nu_L + \nu_1$ and $\nu_L + \nu_3$), the combination of bending and stretching ($\nu_2 + \nu_1, \nu_2 + \nu_3$), and the overtones of the stretching modes ($2\nu_1, 2\nu_3$).²⁵ The first group of such combination bands (i.e., between ν_3 and $2\nu_1$) has been recently observed experimentally using IINS with a very high incident energy.^{17,23} In the region above 6000 cm^{-1} one can notice a sequence of bands which can be assigned to combinations of the fundamental modes of higher order than those discussed above. In all the bands displayed in Fig. 7, the frequency position of the overtones is equal to the sum of the frequencies of the fundamental modes within 0.5%. Thus, at the present temperature, our classical MD simulation suggests that the anharmonicity in the vibrational modes is not significant.

VII. DISCUSSION AND SUMMARY

In this paper we have studied the ice I_h structure of water with the *ab initio* polarizable and flexible NCC–vib potential^{1,4} by performing a molecular dynamics simulation. Compared to static energy minimization and harmonic lattice dynamics techniques, the MD approach has the advantage that anharmonic effects are automatically taken into account. Such anharmonic effects have been shown to be important in the I_h low frequency spectrum.²⁶ Moreover, the low signal-to-noise ratio, which can be obtained in MD simulations, allows the detection of all the overtones and combination bands, with intensities more than 10 orders of magnitude smaller than the strong fundamental peaks.

In agreement with the recent reinterpretation of the neutron scattering data, we find that: (i) the equilibrium position of the oxygen atoms is disordered, an effect related to the disorder in the proton position imposed by the ice rules; (ii) the OH bond length of 0.978 \AA does not change much when comparing the liquid with the solid phase. Discrepancies are instead observed for the HH distance, 0.04 \AA smaller than the value suggested by the NMR data,¹⁰ and for the molecular dipole moment, 10% larger than the experimental estimate.⁷ We attribute these discrepancies to (i) the large bond polarizability of the NCC–vib potential; (ii) to the absence of coupling between the intermolecular and the intramolecular potentials (indeed, the intermolecular part of the potential was obtained from *ab initio* computation on rigid water dimers and trimers and the intramolecular part from *ab initio* computations on a single water molecule¹); (iii) to the neglect of the quantum corrections, which might be very important because of the delocalization of the protons.

We have also studied the low frequency collective modes in ice I_h . A similar study was performed by Tse *et al.*¹⁹ by using rigid nonpolarizable potentials. The density of states shown in Figs. 3 and 4 for NCC–vib is much closer to the experimental values than the DOS calculated for SPC, MCY, and TIPS2 (see Ref. 19 and 26). This confirms the importance of polarization terms in the molecular interaction potential, in particular for the description of the low frequency collective modes. We find good agreement between simulated and experimental data for the acoustic dispersion relations. The agreement between simulated and experimental data is very good in the (0001) direction (*c* axis) and for the transverse phonons in the (11 $\bar{2}$ 0) and (01 $\bar{1}$ 0) directions. Less satisfactory results are found for acoustic longitudinal phonons whose frequencies are in general 10–20% smaller than the corresponding experimental data. These discrepancies are tentatively assigned to deficiencies of the potential in describing with sufficient accuracy the potential hypersurface that controls the OOO bending modes.

The calculated DOS in the librational and vibrational regions are found in fairly good agreement with the IINS experimental data.^{17,23} Although the position of the vibrational bands are not correctly predicted by the NCC model, the frequency change on going from the gas or the liquid to the solid phase are well reproduced. More com-

plex calculations are underway in this laboratory (i) to derive a potential from *ab-initio* calculations on clusters of flexible water molecules and (ii) to evaluate the relevance of the quantum correction.

ACKNOWLEDGMENTS

We wish to thank Professor E. Clementi and Dr. V. Martorana for helpful suggestions. This work has been carried out with the support of "Regione Autonoma Sardegna."

- ¹G. Corongiu, *Int. J. Quantum Chem.* **42**, 1209 (1992); U. Niesar, G. Corongiu, E. Clementi, G. R. Kneller, and D. Bhattacharya, *J. Phys. Chem.* **94**, 7949 (1990).
- ²M. Sprik and M. L. Klein, *J. Chem. Phys.* **89**, 7556 (1988).
- ³J. Caldwell, L. X. Dang, and P. A. Kollman, *J. Am. Chem. Soc.* **112**, 9144 (1990); P. Cieplak, P. Kollman, and T. Lybrand, *J. Chem. Phys.* **92**, 6755 (1990); S. Kuwajima and A. Warshel, *J. Phys. Chem.* **94**, 460 (1990).
- ⁴G. Corongiu and E. Clementi, *J. Chem. Phys.* **97**, 2030 (1992).
- ⁵For a recent review see W. F. Kuhs and M. S. Lehmann, in *Water Science Reviews*, Vol. 2, edited by F. Frank (University Press, Cambridge, 1986).
- ⁶A. Rahman and F. H. Stillinger, *J. Chem. Phys.* **57**, 4009 (1972).
- ⁷E. Whalley, *J. Glaciology* **21**, 13 (1978).
- ⁸S. W. Peterson and H. A. Levy, *Acta Crystallogr.* **10**, 70 (1957).
- ⁹W. F. Kuhs and M. S. Lehmann, *J. Phys. Chem.* **87**, 4312 (1983).
- ¹⁰E. Whalley, *Mol. Phys.* **28**, 1105 (1974).
- ¹¹R. Chidambaran, *Acta Crystallogr.* **14**, 467 (1961).
- ¹²W. F. Kuhs and M. S. Lehmann, *J. Phys. (Paris)* **48**, C1, 3 (1987).
- ¹³P. W. Deutsch, B. N. Hale, R. C. Ward, and D. A. Reago, Jr., *J. Chem. Phys.* **78**, 5103 (1983).
- ¹⁴For a discussion of the polarizability in water see, for example, E. Clementi, W. Kolos, G. C. Lie, and G. Raghino, *Int. J. Quantum Chem.* **27**, 377 (1980).
- ¹⁵W. E. Thiessen and A. H. Narten, *J. Chem. Phys.* **77**, 2646 (1982).
- ¹⁶A. K. Soper and M. G. Phillips, *Chem. Phys.* **107**, 47 (1986).
- ¹⁷J.-C. Li, J. D. Londono, D. K. Ross, J. L. Finney, S. M. Bennington, and A. D. Taylor, *J. Phys. Condens. Matter* **4**, 2109 (1992); J.-C. Li, D. K. Ross, J. D. Londono, J. L. Finney, A. Kolesnikov, and E. G. Ponyatovskii, in *Physics and Chemistry of Ice*, edited by N. Maneno and T. Hondoh (Hokkaido University Press, Sapporo, 1992).
- ¹⁸J. P. Hansen and I. R. McDonald, in *Theory of Simple Liquids* (Academic, New York, 1986).
- ¹⁹J. S. Tse, M. L. Klein, and I. R. McDonald, *J. Chem. Phys.* **81**, 6124 (1984).
- ²⁰The frequency of the well-resolved longitudinal excitation peaks in $S(k, \omega)$ coincides with the value evaluated calculating $J_k(\omega)$.
- ²¹B. Renker, in *Phonons*, edited by M. A. Nusimovici (Flammarion, Paris, 1971), p. 167.
- ²²R. E. Gagnon, Kiefte Clouter, and M. J. Clouter, *J. Chem. Phys.* **92**, 1909 (1990).
- ²³J.-C. Li and D. K. Ross, in *Physics and Chemistry of Ice*, edited by N. Maneno and T. Hondoh (Hokkaido University Press, Sapporo, 1992).
- ²⁴J. E. Bertie and E. Whalley, *J. Chem. Phys.* **46**, 1271 (1967); M. J. Taylor and E. Whalley, *J. Chem. Phys.* **40**, 1660 (1964).
- ²⁵Note that the value of $2\nu_2$ is very close to ν_1 . This makes ambiguous the association of the high frequency overtones with the fundamental modes.
- ²⁶M. Marchi, J. S. Tse, and M. L. Klein, *J. Chem. Phys.* **85**, 2414 (1986).